

Operational atmospheric and wave modelling in the California's coastline and offshore area with applications to wave energy monitoring and assessment

George Galanis, Menas Kafatos, Peter C. Chu, Nikolaos Hatzopoulos, Evgenia Papageorgiou & Aristotelis Liakatas

To cite this article: George Galanis, Menas Kafatos, Peter C. Chu, Nikolaos Hatzopoulos, Evgenia Papageorgiou & Aristotelis Liakatas (2017): Operational atmospheric and wave modelling in the California's coastline and offshore area with applications to wave energy monitoring and assessment, Journal of Operational Oceanography, DOI: [10.1080/1755876X.2017.1349640](https://doi.org/10.1080/1755876X.2017.1349640)

To link to this article: <http://dx.doi.org/10.1080/1755876X.2017.1349640>



Published online: 18 Jul 2017.



Submit your article to this journal [↗](#)



Article views: 5





View related articles [↗](#)



View Crossmark data [↗](#)



Operational atmospheric and wave modelling in the California's coastline and offshore area with applications to wave energy monitoring and assessment

George Galanis^a, Menas Kafatos^b, Peter C. Chu^c, Nikolaos Hatzopoulos^b, Evgenia Papageorgiou ^a and Aristotelis Liakatas ^a

^aHellenic Naval Academy, Mathematical Modeling and Applications Laboratory, Hatzikiriakion, Piraeus, Greece; ^bSchmid College of Science, Chapman University, Orange, CA, USA; ^cDepartment of Oceanography, Graduate School of Engineering & Applied Science, Naval Postgraduate School, Monterey, CA, USA

ABSTRACT

A new high-resolution operational atmospheric/wave forecasting system for the west coastline of the US, focusing especially to the California near and offshore area, is presented in this work. The new system is the result of the collaboration between two US and one European Universities. It consists of two state-of-the-art numerical prediction models (Regional Atmospheric Modeling System and Wave Model) supported by a new optimisation statistical module for the bias reduction and local adaptation of the results based on non-linear Kalman filtering and Bayesian statistics. The presented system has been evaluated against a wide number of National Data Buoy Center buoys records with very promising results. Moreover, applications to wave energy site assessment are presented revealing areas of the California coastline with increased power potential appropriate for wave power plants installation.

ARTICLE HISTORY

Received 7 July 2016
Accepted 23 June 2017

1. Introduction

In the last decade, Numerical modelling has been proved an excellent alternative to observations for environmental parameters especially over sea regions where the available atmospheric and wave observation networks are not as dense as over land areas. Several types of modelling systems have been proposed targeting not only to the support of operational environmental forecasting (Papadopoulos et al. 2002; Zodiatis et al. 2003, 2008; Papadopoulos and Katsafados 2009, Galanis et al. 2012) but also to important applications, including renewable energy assessment and monitoring (Louka et al. 2008; Defne et al. 2009; Iglesias and Carballo 2009, 2010; Iglesias et al. 2009; Rusu and Soares 2012; Akpınar and Kömürçü 2013; Zodiatis et al. 2014, 2015); pollution monitoring and prevention (Janeiro et al. 2012); desert dust studies (Nickovic et al. 2001; Balis et al. 2006; Spyrou et al. 2010); air-quality modelling (Astitha et al. 2005).

In this work, a new operational forecasting system developed jointly by the Naval Ocean Analysis and Prediction Laboratory of the US Naval Postgraduate School, the Center of Excellence in Earth Systems Modeling & Observations of the Schmid College of Science & Technology, Chapman University, California and the

Mathematical Modeling Laboratory of the Naval Academy of Greece is proposed for covering the west coastline and offshore regions of the US with special emphasis to the California sea area. This system consists of two state-of-the-art numerical models, namely the Regional Atmospheric Modeling System (RAMS) (Kallos and Lagouvardos 1997; Mavromatidis and Kallos 2002; Cotton et al. 2003) and the third-generation Wave Model (WAM) (WAMDIG 1988; Komen et al. 1994; Bidlot et al. 2007), operating, through a sequence of nested domains, at a high-resolution mode reaching a horizontal grid of 2 km in the finer domain. The numerical wind and wave prediction models are supported by an optimisation statistical module based on Kalman filters and Bayesian inference able to detect and reduce potential discrepancies of the initial model outputs due to local peculiarities or other bias generating issues (Galanis and Anadranistakis 2002; Galanis et al. 2006, 2009, 2011; Louka et al. 2008; Pelland et al. 2011).

The three components of the system are coupled, leading to an integrated operational tool able to credibly forecast in detail, and at a very high-resolution mode, critical atmospheric and wave parameters, as an evaluation study against offshore National Data Buoy Center (NDBC) buoys over the west coast line of the US proves.

The obtained results are utilised towards a detailed study of the wave energy potential over the west coastline of the US, providing information for sea areas that favour the development of wave energy platforms spotting, at the same time, possible constraints due to potential extreme weather events impact. In this way, a new integrated system is provided to the research and technical community of environmental modelling, proposing also a potentially helpful tool for decision-makers on renewable energy monitoring and exploitation, able to support site assessment studies for a ‘clean’ form of energy that is available plentiful in California due to the local wave climatology.

2. Models and methodology

2.1. Atmospheric modelling

The RAMS (version 4.3.0 for the current work) is an advanced state-of-the-art numerical code, developed at Colorado State University and Mission Research Inc/ASTeR Division. It combines a non-hydrostatic cloud microphysical process algorithm and a hydrostatic mesoscale model making the system able to simulate atmospheric phenomena with resolution ranging from tens of kilometres to a few metres with a surface parameterisation scheme utilising information on land-use and soil texture at subgrid scale.

RAMS is well parallelised, avoiding the use of global physical or numerical routines. It is utilised today for operational and research purposes by a wide number of leading institutes worldwide. A general description of the model capacities and developments can be found in Cotton et al. (2003); Kallos and Lagouvardos (1997) and Mavromatidis and Kallos (2002).

The model has been employed with two-way interactive nesting option for any number of grids. The system developed at the Center of Excellence in Earth Systems Modeling & Observations in Chapman University consists of a sequel of three domains presented in detail in Table 1. The first covers the major South West coastline of the US at a horizontal resolution of 24 km, the second is focusing to the California region at 6 km and a third high-resolution (2 km) nested domain is covering the

Table 1. The configuration of the three sequel atmospheric model domains.

| | Coarse | First nest | Second nest |
|-----------------------|-------------------|--------------------|--------------------|
| Longitude | 127.89W to 08.11W | 120.99W to 115.01W | 120.06W to 117.92W |
| Latitude | 26.54N to 41.69N | 31.81N to 36.65N | 33.36N to 35.12N |
| Horizontal resolution | 24 km | 6 km | 2 km |

greater LA region (Figure 1). In the vertical, RAMS integrates at 32 levels.

It is of importance here to briefly discuss the local climate of the study area. Climate features of the Southern California are classified as belonging to the Mediterranean Dry Summer Subtropical climatic type, with a cool summer regime. Temperatures, along the maritime fringe, are controlled by the sea. The warm month average is below 72°F, while the cold month average is above 50°F. Precipitation is strongly concentrated in winter, with average annual values in the vicinity of 15 inches (Dailey et al. 1974).

California state waters extend from the shoreline to three nautical miles offshore, and this nearshore area is advantageous for renewable energy technology applications due to logistical and economic reasons (Harvey and Nelson 2008). The oceanographic features of Southern California occur due to its location, the eastern boundary of the North Pacific Ocean. The surface water seaward of the offshore islands moves south with the eastern boundary current, the California Current. A southerly current flows north below the Californian Current, and a southerly surface countercurrent occurs landward of the California Current. Seasonal coastal upwelling, mixed semidiurnal tides and wave motion cause distinct circulation patterns in the littoral zone (Dailey et al. 1974).

2.2. Wave modelling

The accurate prediction of sea waves over the coastline and offshore area of California was one of the main objectives of the presented operational system. As a result, the choice of a well-established wave model, able

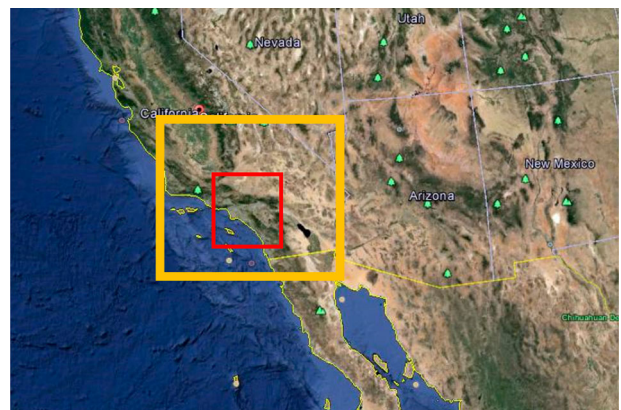


Figure 1. The domains of the atmospheric model RAMS. The orange rectangle defines the borders of the first nested domain covering the southern California area at a horizontal resolution of 6 km while the red one the subsequent finer nested area focusing to the major Los Angeles region at a very high horizontal resolution of 2 km.

to successfully simulate different wave types, was critical. For these reasons, the third-generation wave model WAM (WAMDIG 1988; Komen et al. 1994; Bidlot et al. 2007) was selected as a well-tested and evaluated model utilised today by a wide number of operational and research centres worldwide.

WAM is based on the numerical solution of the wave transport equation explicitly without adopting any specific shapes or types of the 2d – over frequencies and directions – wave spectrum:

$$\frac{dF}{dt} + \frac{\partial}{\partial \phi}(\dot{\phi}F) + \frac{\partial}{\partial \lambda}(\dot{\lambda}F) + \frac{\partial}{\partial \theta}(\dot{\theta}F) = S,$$

where F represents the spectral density with respect to frequencies (f), directions (θ), latitudes (ϕ) and longitudes (λ). The source function S components include the wind forcing, white capping dissipation and non-linear transfer.

More precisely, in our study, the ECMWF version, CY36R4 (Jansen 2000, 2004) was adopted. This version is enhanced with critical updates, including a new advection scheme able to take into account contributions from the corner points (Bidlot et al. 2007), new extreme wave parameters – namely the average maximum wave height and the corresponding wave period (Mori and Janssen 2006) based on the determination of the kurtosis of the wave field (Janssen and Onorato 2007), as well as a new parameterisation of shallow water effects which provides the option to simulate equally well over offshore deep water areas and near shore shallow water environments. It should be also noted that in the wind/wave models utilised in the present

work no data assimilation has been employed. This was mainly imposed by the version of the wave model adopted, in which the data assimilation scheme was not fully integrated, and by the operational type of the modelling system and the data access limitations that prevented them from being available at the time of system run.

This new version of the wave model has been already successfully utilised and evaluated in previous studies (Bidlot et al. 2007; Galanis et al. 2011, 2012; Bidlot 2012; Emmanouil et al. 2012, 2016; Zodiatis et al. 2015). A detailed evaluation for the presented operational system also follows in the next sections.

The wave model was operated on a sequel of three domains covering the whole west coast of the US and then focusing on the California offshore area, as depicted in Figure 2.

The first nested domain (red rectangle in Figure 2) takes boundary conditions from a global version of the wave model that operates at a horizontal resolution of 0.5° forced by the Global Forecast System (GFS) atmospheric model. In this way all the necessary swell information that affects the region of interest is taken into account. WAM runs at a horizontal resolution of 0.1 × 0.1° in the ‘red’ area, while the wave spectra are discretised to 30 frequencies (range 0.0417–0.6626 Hz logarithmically spaced) and 24 directions (equally spaced). In this way, swell waves up to 24 s can be successfully simulated covering any possible wave conditions in the east part of the Pacific Ocean and being at the same time in accordance with the limit of wave buoys utilising accelerometers. Wind forcing in this domain is also

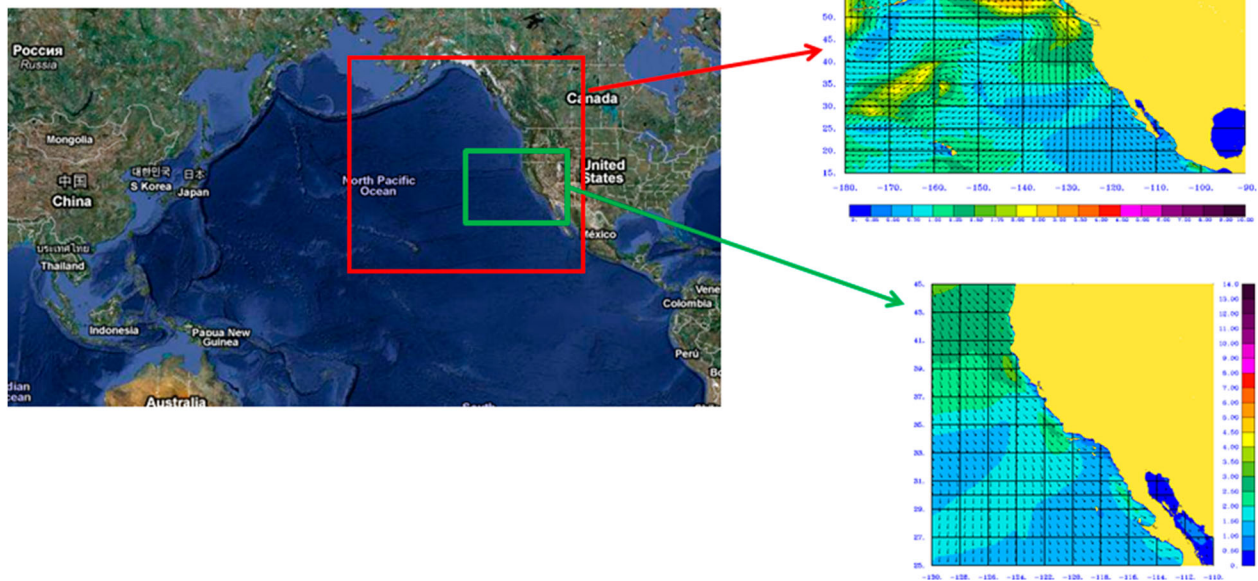


Figure 2. The domains of the wave model WAM. The red rectangle defines the borders of the first nested domain covering the Eastern part of the Pacific Ocean and the West US coastline at a horizontal resolution of 0.1° while the green one the subsequent nested region focusing to the SW US coastline at a very high horizontal resolution of 0.01667°.

provided by GFS in conjunction with the RAMS atmospheric model.

A similar configuration has been also adopted in the second, finest nested domain – the green one in Figure 2 – where a high horizontal resolution of $0.01667 \times 0.01667^\circ$ has been adopted. The wind forcing here is obtained by the finest available domain of the atmospheric model RAMS described in the previous subsection. In areas that are not covered by RAMS, wind forcing from the National Centers for Environmental Prediction GFS model is utilised for driving the wave model as presented in Table 2. In the boundary areas between the two atmospheric models, a merging system is employed in order to smooth possible gradients, which, in any case, are not likely since the two atmospheric models are not independent: GFS provides boundary and lateral conditions to RAMS.

This is a one-way coupled system where the atmospheric model outputs are used as forcing for the wave model. It should be noted, however, that the atmospheric system, apart from the necessary input for the wave system, supports as a standalone system the operational atmospheric forecast provided by the Schmid College of Science, Chapman University.

Bathymetric data were obtained from US National Geophysical Data Center's (NGDC) ETOPO-1 data set providing a 1 arc-minute gridded information.

It is worth to notice at this point that although the basic parameter integrated by the wave model is the 2d wave spectrum $F(f, \theta, \varphi, \lambda)$, as defined above, the main necessary parameters for applications, including renewable energy activities discussed in Section 4 of our study, are the significant wave height H_s and the mean wave period T_e . Both can be obtained by the moments of the 2d wave spectrum:

$$H_s = 4\sqrt{m_0}, \quad T_e = \frac{m_{-1}}{m_0},$$

where

$$m_n = \int_0^{2\pi} \int_0^\infty f^n F(f, \theta) df d\theta, \quad n = -1, 0, 1.$$

2.3. A hybrid Bayesian–Kalman filter post processing

The numerical atmospheric–wave model presented in the previous subsections is followed up by an advanced post-processing system that supports the local adaptation of the direct model outputs. Such systems are indispensable parts in today's integrated operational forecasting platforms since they can contribute in well-known shortcomings of numerical models. The latter, when exploited for local forecasts, usually exhibit systematic or more complicated types of discrepancies especially when focusing to near-surface or surface parameters: wind speed and wave heights are particularly exposed to such type of problems as a result of contributing factors; smoothing in landscape characteristics, certain parameterisation, sub-scale phenomena, lateral and boundary condition problems can be listed among them (see e.g. Janjic 1994; Rao et al. 1997; Galanis and Anadranistakis 2002; Kalnay 2002; Mass et al. 2002; Emmanouil et al. 2006; Galanis et al. 2006, 2009, 2011; Louka et al. 2008; Stathopoulos et al. 2013).

In the presented integrated operational system, a Bayesian–Kalman-based post-process model has been chosen. The latter has been proved able to almost eliminate systematic biases from the direct model outputs but also to critically reduce the error variability and the associated forecasting uncertainty. More precisely, the model bias y_t is estimated by means of a non-linear polynomial based on the direct model output m_t that results to the observation equation of the Kalman filter:

$$y_t = x_{0,t} + x_{1,t} \cdot m_t + x_{2,t} \cdot m_t^2 + \dots + x_{n,t} \cdot m_t^n + v_t,$$

where the weights $x_{i,t}$ form the state vector $x_t = [x_{0,t} \ x_{1,t} \ x_{2,t} \ \dots \ x_{n,t}]$ of the filter, satisfying the corresponding system equation:

$$x_t = x_{t-1} + w_t.$$

The optimum degree of the employed polynomial depends on the specific parameter as well as on the

Table 2. The configuration of the wave model WAM.

| Wave model | WAM, ECMWF version CY36R4 | | |
|------------------------|--|---|--|
| Area covered | Global Lat range: 80S–80N Lon range: 180W–180E | East Pacific Lat range: 15N–60N Lon range: 180W–90W | SW US offshore and coastline Lat range: 25N–45N Lon range: 130W–110W |
| Horizontal resolution | 0.5 × 0.5° | | |
| Frequencies | 30 (range 0.0417–0.6626 Hz logarithmically spaced) | 30 (range 0.0417–0.6626 Hz logarithmically spaced) | 30 (range 0.0417–0.6626 Hz logarithmically spaced) |
| Directions | 24 (equally spaced) | 24 (equally spaced) | 24 (equally spaced) |
| Time step | 300 s | 150 s | 50 s |
| Wind forcing | GFS atmospheric model | GFS and RAMS atmospheric models | GFS and RAMS atmospheric models |
| Wind forcing time step | 6 h | 1 h | 1 h |
| Bathymetry | US-NGDC ETOPO1 data set 0.01667 × .001667° | | |

time and space under study. More information and applications of the classical Kalman filter theory can be found in Kalman (1960); Kalman and Bucy (1961); Kalnay (2002); Crochet (2004); Galanis et al. (2006, 2009, 2011); Louka et al. (2008); Pelland et al. (2011) and Stathopoulos et al. (2013).

The remaining non-systematic errors v_t and w_t are elaborated by a follow-up linear Bayesian model. In particular, two approaches are adopted based on the optimum distribution fitted to the parameter under study which, in the vast majority of the study cases (see for example Ferreira and Soares 1999, Galanis et al. 2012), is the Normal, the Weibull or the Lognormal (LN) distribution.

In the former case, the probability density functions of non-systematic part of the error v_t and the corresponding observations o_t are the Gaussians $N(0, \sigma_v^2)$ and $N(o_\mu, \sigma_o^2)$, respectively. On the other hand, for the conditional pdfs of the Kalman filter outputs k_t , the Bayesian theory (Box and Tiao 1992; Bernardo and Smith 2000) gives that

$$P(k_t|o_t) = N(o_t, \sigma_v^2),$$

$$P(o_t|k_t) \propto P(k_t|o_t)P(o_t),$$

$$P(o_t|k_t) \propto e^{-(k_t-o_t)^2/2\sigma_v^2} e^{-(o_t-o_\mu)^2/2\sigma_o^2} \Rightarrow P(o_t|k_t) \sim N(\mu, \sigma^2),$$

where

$$\mu = \left(k_t \frac{1}{\sigma_v^2} + o_\mu \frac{1}{\sigma_o^2} \right) / \left(\frac{1}{\sigma_v^2} + \frac{1}{\sigma_o^2} \right) \quad \text{and}$$

$$\sigma = \left(\frac{1}{\sigma_v^2} + \frac{1}{\sigma_o^2} \right)^{-1}.$$

Based on this, the final forecast provided by means of the maximum a posteriori estimator is

$$\hat{o}_t = \operatorname{argmax} P(o_t|k_t).$$

On the other hand, when the data under study are better described by a skewed distribution – like many times is noticed for wind speed (see for example Zodiatis et al. 2014; Emmanouil et al. 2016), then the Weibull distribution is employed under the following assumptions for the corresponding pdfs of the non-systematic part of the error v_t and the observations o_t : $P(o_t) = W(a, b)$, $P(v_t) = N(0, \sigma^2)$.

The posterior distributions take then the following form:

$$P(o_t|k_t) = \frac{(1/\sqrt{2\pi\sigma^2}) e^{-(k_t-o_t)^2/2\sigma^2} (a/b)(o_t/b)^{(a-1)} e^{-(o_t/b)^a}}{\int (1/\sqrt{2\pi\sigma^2}) e^{-(k_t-o_t)^2/2\sigma^2} (a/b)(o_t/b)^{(a-1)} e^{-(o_t/b)^a} do_t}$$

$$\Rightarrow P(o_t|k_t) = \frac{e^{-(k_t-o_t)^2/2\sigma^2} o_t^{(a-1)} e^{-(o_t/b)^a}}{\int e^{-(k_t-o_t)^2/2\sigma^2} o_t^{(a-1)} e^{-(o_t/b)^a} do_t}.$$

and the final forecast is given by the corresponding posterior mean

$$E(o_t) = \frac{\int e^{-(k_t-o_t)^2/2\sigma^2} o_t^a e^{-(o_t/b)^a} do_t}{\int e^{-(k_t-o_t)^2/2\sigma^2} o_t^{(a-1)} e^{-(o_t/b)^a} do_t}.$$

On the other hand, the wave height data are also well described in many cases by the LN distribution. In this framework, the probability density function of non-systematic part of the error v_t is the Gaussian $N(0, \sigma^2)$, while the corresponding observations o_t are distributed by $\text{LN}(o_\mu, \sigma_o^2)$.

The posterior distributions then take the following form:

$$P(o_t|k_t) = \frac{(1/o_t) e^{-((k_t-o_t)^2/2\sigma^2 + (\ln o_t - o_\mu)/2\sigma_o^2))}}{\int (1/o_t) e^{-((k_t-o_t)^2/2\sigma^2 + (\ln o_t - o_\mu)/2\sigma_o^2))} do_t},$$

and the prediction is given by the corresponding posterior mean

$$E(o_t) = \frac{\int e^{-((k_t-o_t)^2/2\sigma^2 + (\ln o_t - o_\mu)/2\sigma_o^2))} do_t}{\int (1/o_t) e^{-((k_t-o_t)^2/2\sigma^2 + (\ln o_t - o_\mu)/2\sigma_o^2))} do_t}.$$

For more details on the specific model, the reader is referred to Galanis et al. (2017), and for the general Bayesian modelling theory, to Box and Tiao (1992) and Bernardo and Smith (2000).

3. Evaluation of the operational system

Our main goal in this section is to evaluate the performance of the integrated atmospheric/wave system focusing on those parameters that are critical both for the general performance of the models and for the estimation of wave energy potential in the area, presented in Section 4: the wave height, the wind speed and the peak wave period.

The wind and wave modelled data have been evaluated against the NDBC Stations (Figure 3) for a time period of five years (2010–2014), in a pseudo-operational mode: Available observations are compared with model forecasts over moving 24-h windows.

The validation analysis has been based on the following statistical indexes, with *obs* denoting the observations

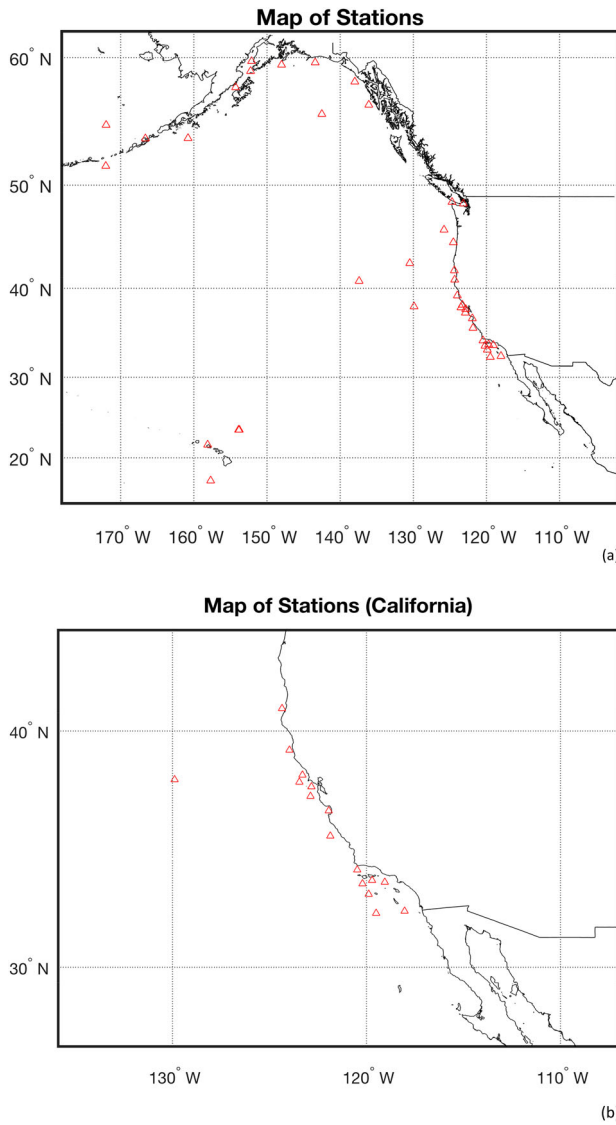


Figure 3. (a) Buoy/meteorological stations used for the evaluation of the operational system and (b) Buoy/meteorological stations employed in the area of application (California).

and mod the corresponding modelled data, while N stands for the sample size:

$$\text{BIAS: } \frac{1}{N} \sum_{i=1}^N (\text{obs}_i - \text{mod}_i),$$

revealing possible systematic deviations of the modelling system.

$$\text{Normalized Bias(NBIAS): } \frac{1}{N} \sum_{i=1}^N \frac{\text{obs}_i - \text{mod}_i}{\text{obs}_i},$$

estimating the model discrepancies as a percentage of the observations. This is an important statistical value for the general evaluation of the modelling system when taken into account in conjunction with absolute bias values.

However, for wave production, the absolute bias values remain more important.

$$\text{Root Mean Square Error(RMSE): } \sqrt{\frac{\sum_{i=1}^N (\text{obs}_i - \text{mod}_i)^2}{N}},$$

characterising the variability of the error.

Nash–Sutcliffe efficiency coefficient (NS):

$$\text{NS} = 1 - \frac{\sum_{i=1}^N (\text{obs}_i - \text{mod}_i)^2}{\sum_{i=1}^N (\text{obs}_i - \bar{O})^2},$$

where \bar{O} denotes the mean value of the observations as a reference value.

Correlation coefficient (R) between modelled and recorded values:

$$R = \frac{\sum_{i=1}^N (\text{mod}_i - \overline{\text{mod}})(\text{obs}_i - \overline{\text{obs}})}{\sqrt{\sum_{i=1}^N (\text{mod}_i - \overline{\text{mod}})^2} \cdot \sqrt{\sum_{i=1}^N (\text{obs}_i - \overline{\text{obs}})^2}},$$

a measure of their linear correlation.

Scatter Index (SI):

$$\text{SI} = \frac{\text{RMSE}}{\text{Observation mean}},$$

which gives the Root Mean Square Error (RMSE) normalised by the observation mean.

Percentiles of model outputs and observations, which provide a complete view of the general distribution of the data.

It is important to mention at this point that the evaluation procedure was taken place after the optimisation post-process on a pseudo-operational mode. More precisely, for the day of operational run T0, the post-processing training period was that of previous days T(-1) to T(-7). The optimisation system, with the obtained from the seven previous days' weights, was then applied to the modelled/forecasted data of the current and subsequent days of forecasts T0–T3. The observations corresponding to day T0 were afterwards employed only for evaluation of the system results for day T0, ensuring in this way that no observation data were used for training and evaluation simultaneously. This operational cycle was repeated for the next day of forecast.

It is worth also to notice that the timing of events is taken into account by the above statistical indexes since the modelled (mod_i) and observation (obs_i) values correspond to the same time. Moreover, the obtained statistics have been estimated over each buoy location differently.

Beginning the analysis with the significant wave height, a crucial parameter for the applications and characteristic for model's efficiency, the average values

Table 3. Averaged values of statistical indexes for the sig. wave height.

| | Statistical indexes values for sign. wave height | | | | | |
|-----------------|--|-----------|------|------|------|--------|
| | BIAS | NBIAS (%) | RMSE | NS | R | SI (%) |
| All stations | -0.04 | -5.30% | 0.66 | 0.39 | 0.75 | 28.54 |
| California area | -0.02 | -5.35% | 0.62 | 0.23 | 0.68 | 33.11 |

of statistical indexes comparing data from all stations (line 1) and for the California area (line 2) are presented in Table 3. The results, for both groups, indicate a very satisfactory general behaviour of the model compared to observation data. BIAS and NBIAS are significantly low, proving that the forecasted values of significant wave height are very close to observations, and RMSE index illustrates the limited variability. Moreover, the values of NS and R indexes further confirm this tendency to reliable predictions, despite the medium linear correlation spotted by the average value of index R. This is something spotted by previous works too, engaging Kalman filters, the utilisation of which may result to a radical reduction of biases leading, on the other hand, to an increased phase noise (see for example Galanis et al. 2006, Louka et al. 2008).

Histograms of NBIAS distribution, presented in Figure 4, point out that the model differentiates from observations at a rate of less than 10% to the vast majority of stations, which is more than 80% of them. The cases with increased percentage of deviation (areas -60 to -70 and -40 to -30) are in fact critically limited and cannot be attributed to certain synoptic situations but rather to model or station outliers. Focusing in the area between -10% and 0 deviations, it should be noted that most of the results are at rates lower than 8%.

Additionally, the histogram of RMSE distribution reveals values less than 0.8 to nearly 90% of stations

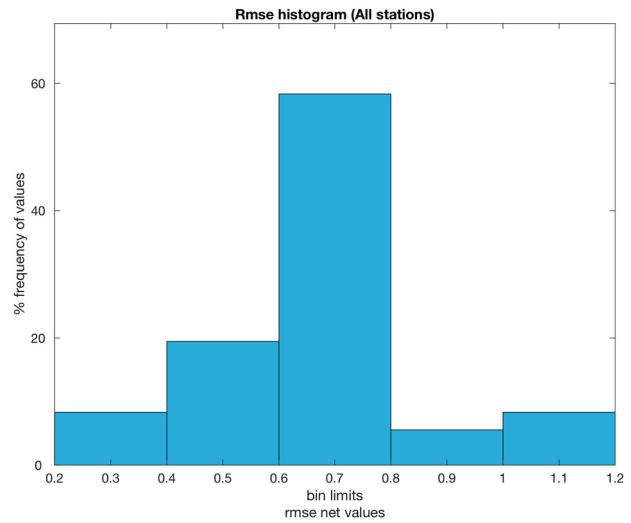


Figure 5. RMSE histogram for all stations (sig. wave height).

under study – a fact underlying the very limited variability of the model errors (Figure 5).

On the other hand, the general distribution of modelled and observed wave height data are presented in the percentiles and scatter diagrams (Figures 6–8) for indicative cases of stations. Slight variations of the model in comparison to the observations are only recorded.

Trying to spot and analyse some of the cases where the model presents noticeable deviations, one could refer to the stations 46047 and 46069, where the model overestimates the observations, especially the maximum values (Figure 7).

In particular, in these cases the model overestimates maximum values with increased variation, overestimates or underestimates the intermediate values with lower variations and overestimates or underestimates the minimum values with small variations.

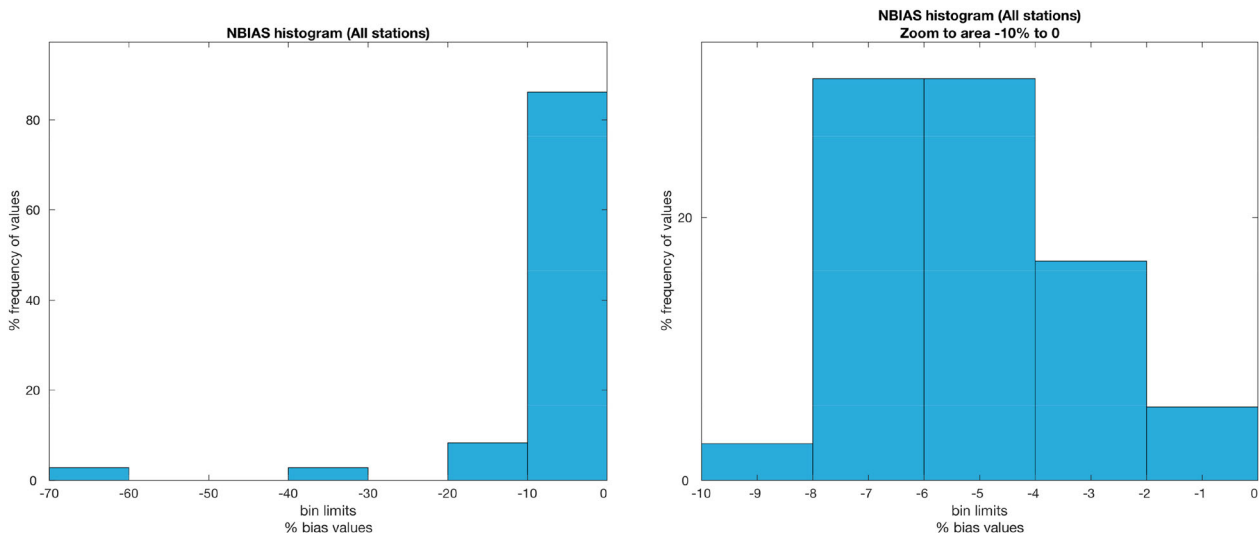


Figure 4. Histograms of NBIAS for all stations and zoomed to values between -10% and 0 (sig. wave height).

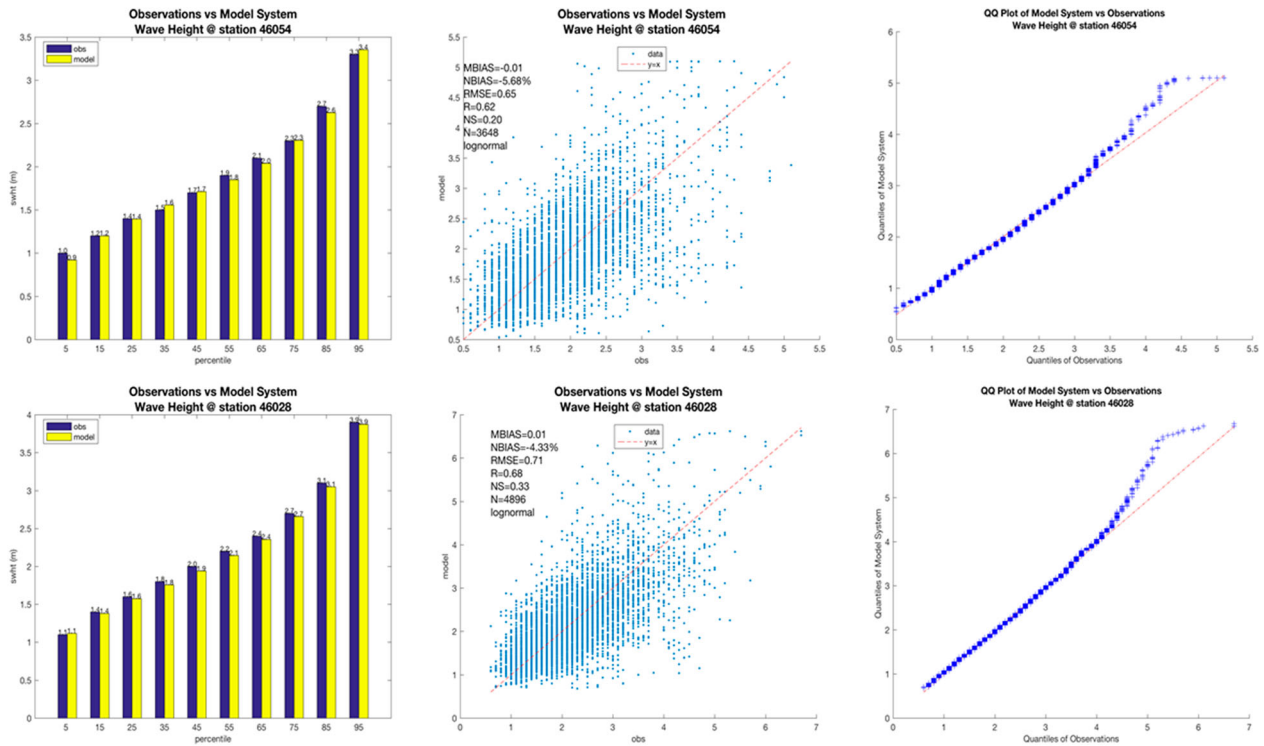


Figure 6. Percentiles, scatter diagrams and QQ plots for observations and model. NDBC stations 46054 and 46028 (sig. wave height).

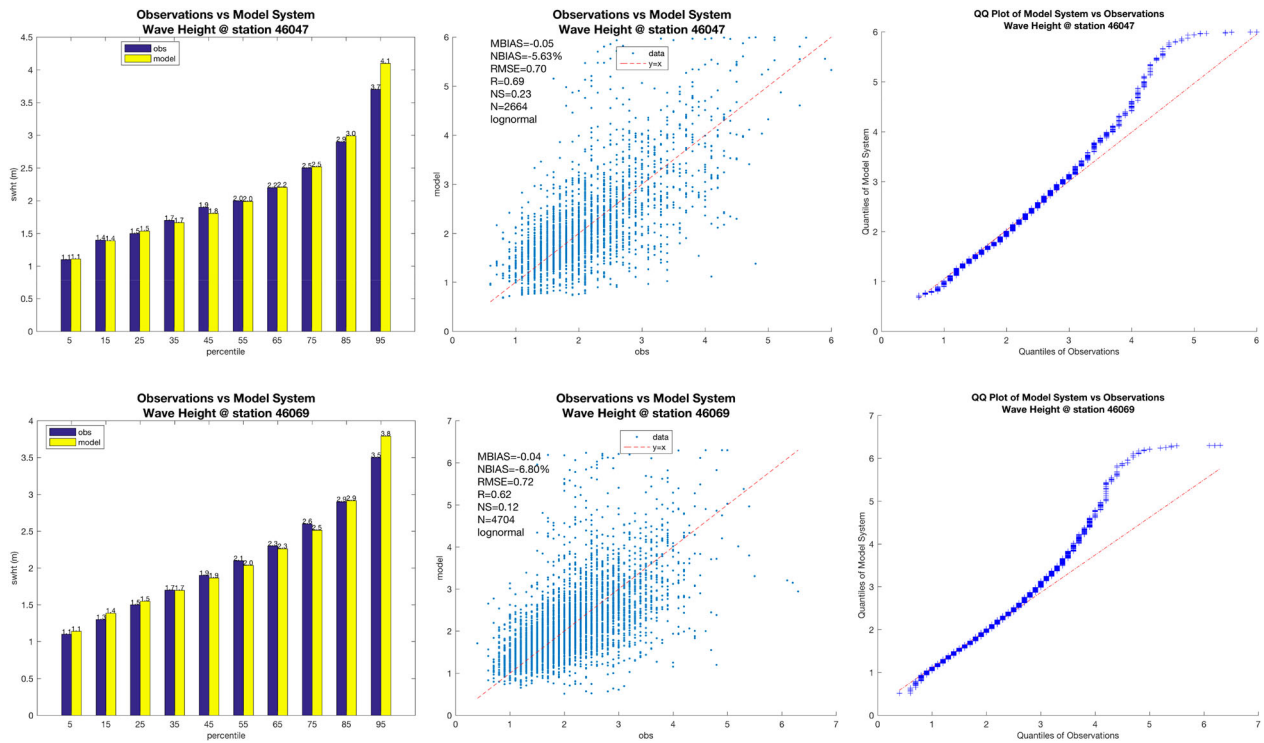


Figure 7. Percentiles, scatter diagrams and QQ plots for observations and model. NDBC stations 46047 and 46069 (sig. wave height).

Since extreme values' estimation is always an important issue for operational forecasting systems led us to dig deeper presenting the model discrepancy rates on maximum values of wave height, as

estimated by the 95th percentile from all stations (Table 4). The model seems to overestimate in most of the cases (80.9%); however the magnitude of this overestimation is

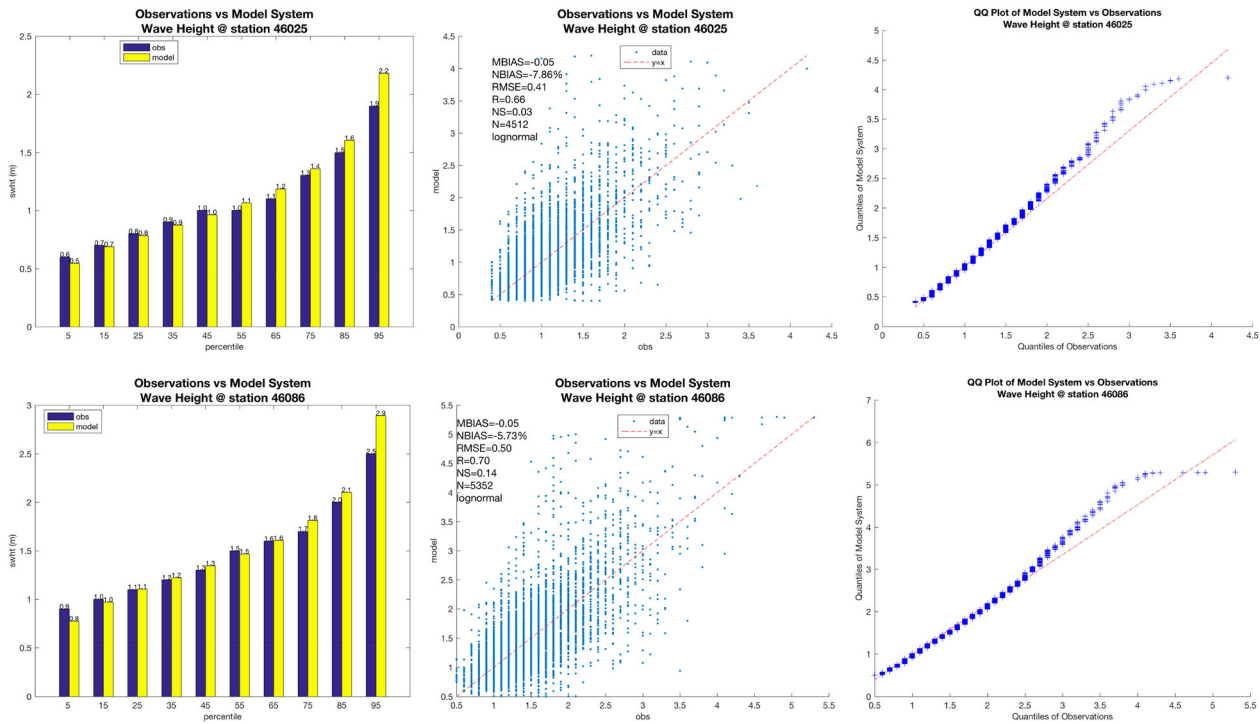


Figure 8. Percentiles, scatter diagrams and QQ plots for observations and model. NDBC stations 46025 and 46086 (sig. wave height).

Table 4. Analysis of the cases where the wave model differentiates significant wave heights.

| | | | | | | | |
|--|--------------|-------------|----------|---------|-----------|-----------|-----------|
| Rate of discrepancy (model – observations) | -40% to -20% | -10% to -2% | -2% to 0 | 0 to 2% | 2% to 10% | 10 to 20% | 20 to 30% |
| Percentage of stations | 5.4% | 2.7% | 10.8% | 10.8% | 45.8% | 21.6% | 2.7% |

Table 5. Averaged values of statistical indexes for wind speed.

| | Statistical indexes values for wind speed | | | | | |
|-----------------|---|-----------|------|------|------|--------|
| | BIAS | NBIAS (%) | RMSE | NS | R | SI (%) |
| All stations | 0.07 | -15.12 | 2.33 | 0.46 | 0.77 | 37.73 |
| California area | 0.29 | -18.46 | 3.06 | 0.09 | 0.50 | 44.74 |

limited to less than 10% in 55+ % of the cases. Of course, for an operational forecasting system, it is always preferable to overestimate than underestimate the significant wave height for extreme wave events and natural hazards, but it is the opposite for resource assessment. Therefore, the goal here is an accurate as possible forecasting system that could equally support everyday activities and resource studies.

In general, it is important to note that at 21.6% of the stations the predictions differentiate less than 2% from the observations.

Concerning the evaluation of wind speed and direction, the successful performance of the model is reconfirmed as the statistical indexes employed prove (Table 5).

Discrepancies between observations and forecasts are minimum, as it is indicated by BIAS values. On the other hand, low variation is shown by RMSE. NS and linear

correlation indexes are also within acceptable limits. As it is expected, the statistics are improved when including in the analysis the offshore stations (all stations category) where the spatial and temporal evolution of wind speed is much smoother and, therefore, more easily predicted. The increased NBIAS comparing to the corresponding value for H_s underlines the fact that in a swell-dominated area, as the one under study, the prediction of winds is always an issue of increased difficulty.

In Figures 9 and 10, representative cases of the wind speed modelled and observed distributions are displayed.

It is worth noticing at this point that the atmospheric model captures almost perfectly the wind direction in cases where a specific pattern of wind behaviour is present.

Finally, peak wave period forecasts are evaluated against observations from NDBC buoys. In all cases where noticeable deviations emerged the hybrid Bayesian-Kalman filter presented in previous sections is activated. The main results, for the whole area covered by the operational system and the major California area, are summarised in Table 6.

The nature of this parameter makes it extremely spatially sensitive a fact that, at least partly, explains

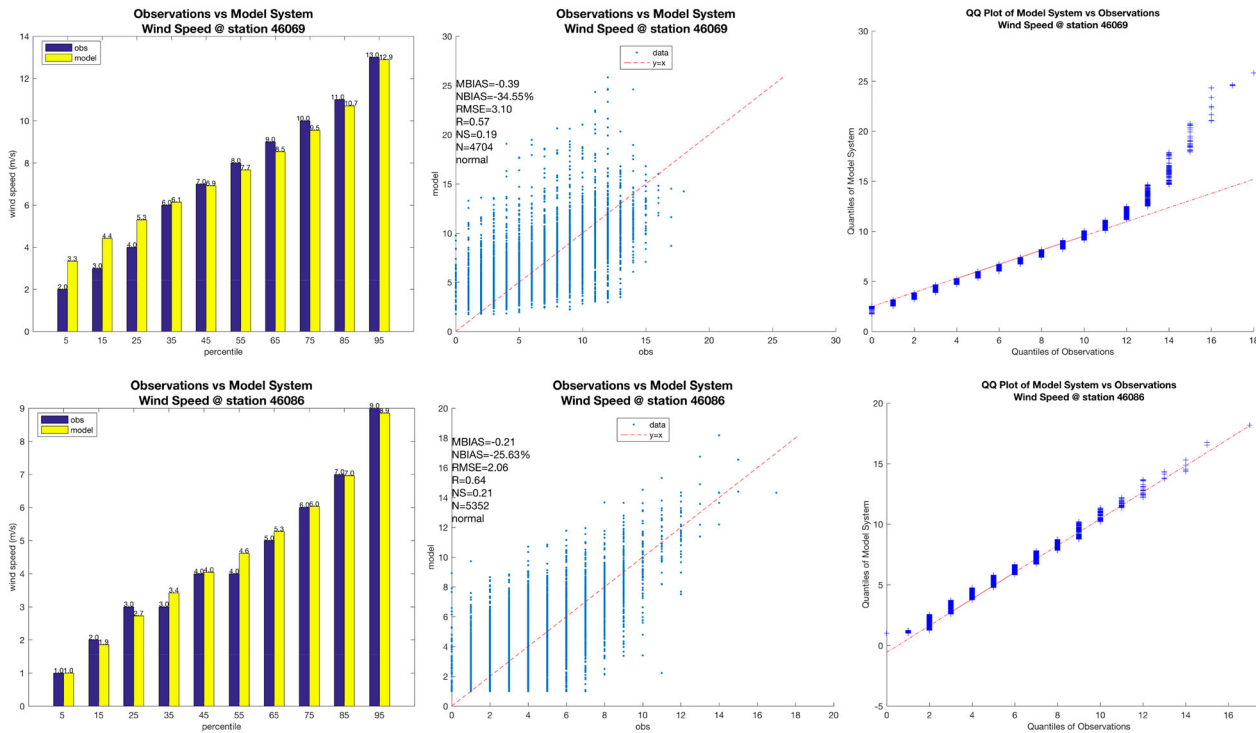


Figure 9. Percentiles, scatter diagrams and QQ plots for observations and model. NDBC stations 46069 and 46086 (wind speed).

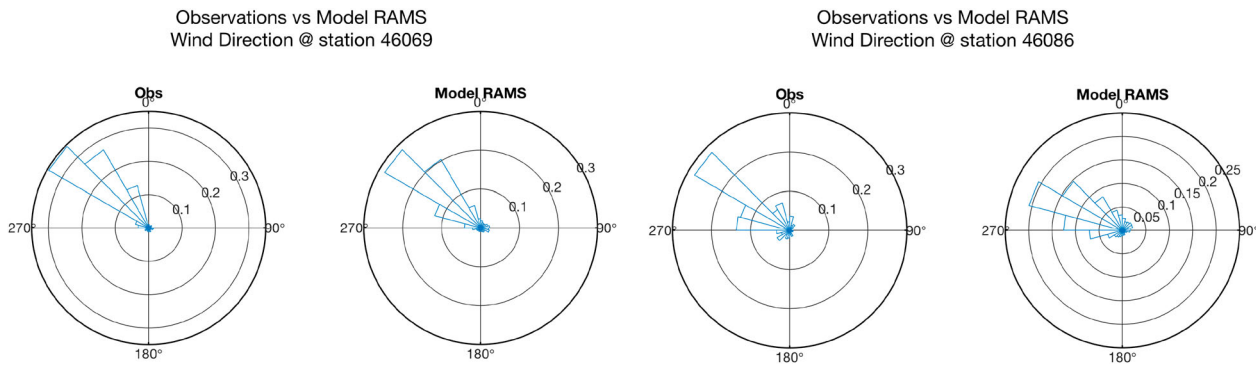


Figure 10. Wind rose diagrams for observations and model. NDBC stations 46069 and 46086 (wind direction).

Table 6. Averaged values of statistical indexes for peak wave period.

| Statistical indexes values for peak wave period | | | | | | |
|---|------|-----------|------|-------|------|--------|
| | BIAS | NBIAS (%) | RMSE | NS | R | SI (%) |
| All stations | 0.05 | -7.00 | 2.94 | 0.01 | 0.32 | 28.18 |
| California area | 0.17 | -6.23 | 3.40 | -0.03 | 0.31 | 29.18 |

the low linear correlation with modelled values. The other statistical indexes however remain at satisfactory levels.

It should be noted that differences and variation between observations and final forecasted values are kept at a desirable level.

As it is displayed in the above representative figures (Figure 11), the model is quite accurate in

the mid values of peak period while slightly overestimating lower extremes and underestimating highest values.

The successful evaluation of the wave period presented, in addition to that of significant wave height, supports quite strongly the well performance of the model over both windwave and swell components of the waves. For the specific area of study, however, it is quite clear that the swell component is the dominant one.

4. Applications on wave energy estimation

The operational system presented in the previous sections is being applied for the estimation of a rising

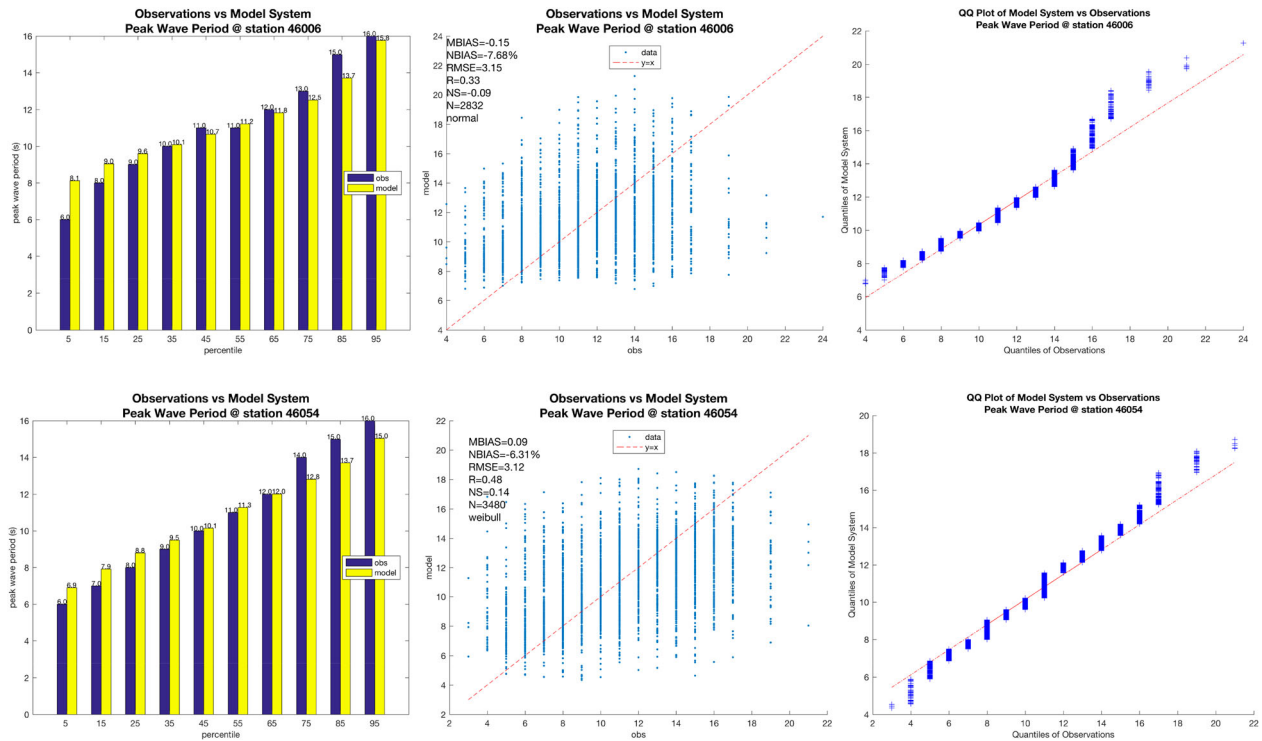


Figure 11. Percentiles, scatter diagrams and QQ plots for observations and model. NDBC stations 46006 and 46054 (peak wave period).

renewable energy source in the California coastline: the wave energy. Apart from the general discussion on renewable resources for energy production, which is receiving increased attention the last years within the new framework posed by the global economic crisis and the security problems concerning the nuclear energy, ocean waves is a source of special interest. This is particularly true for the west coastline of the US due to the continuous wave circulation in Pacific Ocean. California is an even more advantageous case since the wave energy is available closer to the shore, making it cheaper to install and maintain. It should be also noted that California's energy needs are increasing annually at a percentage of 1.25 while only a limited portion of the electricity is obtained from renewable sources.

There are a number of critical advantages of this type of renewable energy comparing to other sources such as the wind power and the photovoltaic potential:

- It is easily adopted to the general grid due to its limited variability.
- Wave power can be produced even in the absence of local winds by exploiting the swell component of the waves.
- Ecological damages or consequences appear negligible (Harvey and Nelson 2008).

Despite these advantages, the exploitation of ocean wave energy still takes the very first steps in US, leaving space for new investments and opportunities while, at the same time, it is one of the hottest topics in Europe.

In this work, we present a detailed analysis of the wave power potential (P) over the South West coastline of the US as well as of the main environmental parameters that affect it: the significant wave height (H_s) and the mean (energy) wave period (T_e). More precisely, P can be estimated based on the following formula:

$$P = \frac{\rho \cdot g^2}{64\pi} H_s^2 T_e,$$

where ρ denotes the water density and g the gravity acceleration. In the present study, the wave modelled data over a period of three years 2012–2015, provided by the integrated modelling system presented in the previous sections, have been utilised for the temporal-spatial analysis of the wave energy potential and the associated wave parameters. The combination of two state-of-the-art high-resolution numerical modelling systems supported by the hybrid optimisation statistical post-process resulted in credible and detailed data for analysis, keeping however in mind that the time length of the selected period is rather short comparing to 10+ years that is commonly utilised to capture interannual variability and therefore the long-term corresponding results for

the estimation of this type of variability could be a bit different.

In Figures 12–19 the spatial distribution of the first four statistical moments, namely the mean value, the

standard deviation, the skewness and the kurtosis, of H_s and T_e are presented for the coastline of California over different seasonal intervals. In this way, information is provided not only for the average behaviour of the

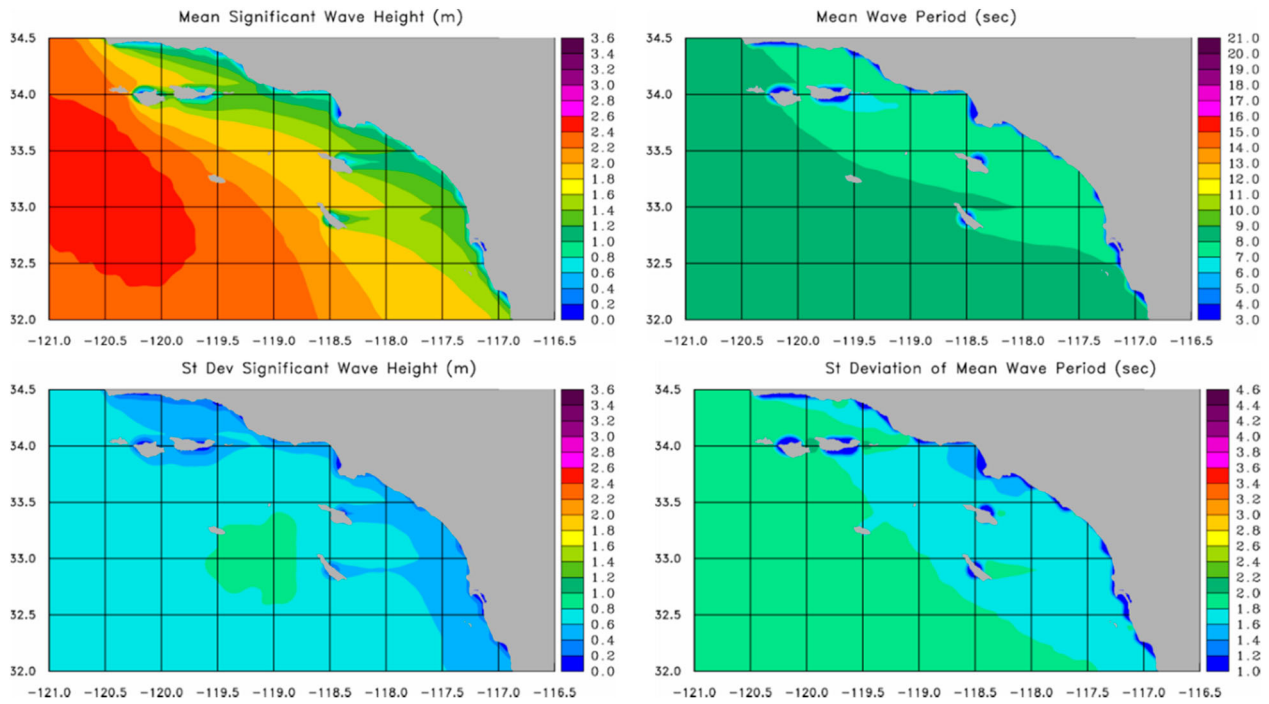


Figure 12. Mean and standard deviation values of the significant wave height and mean wave period for the spring period (March–May).

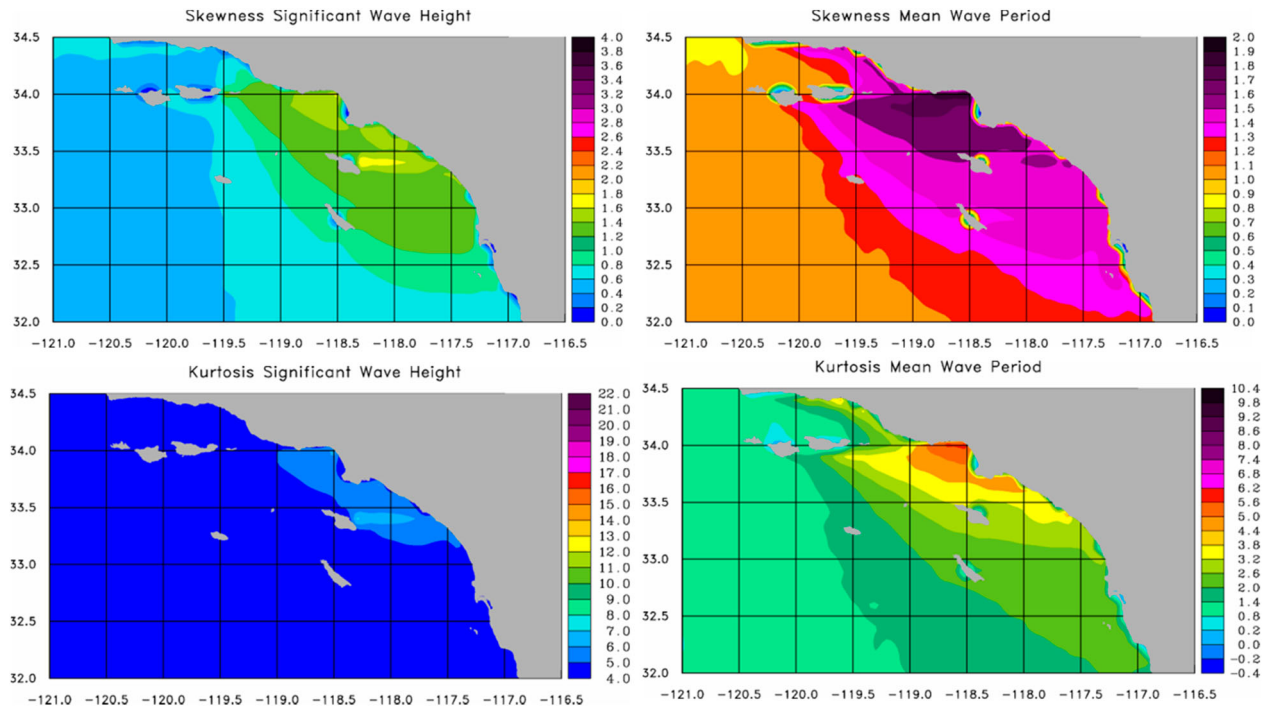


Figure 13. Asymmetry (skewness) and kurtosis measures of the significant wave height and mean wave period for the spring period (March–May).

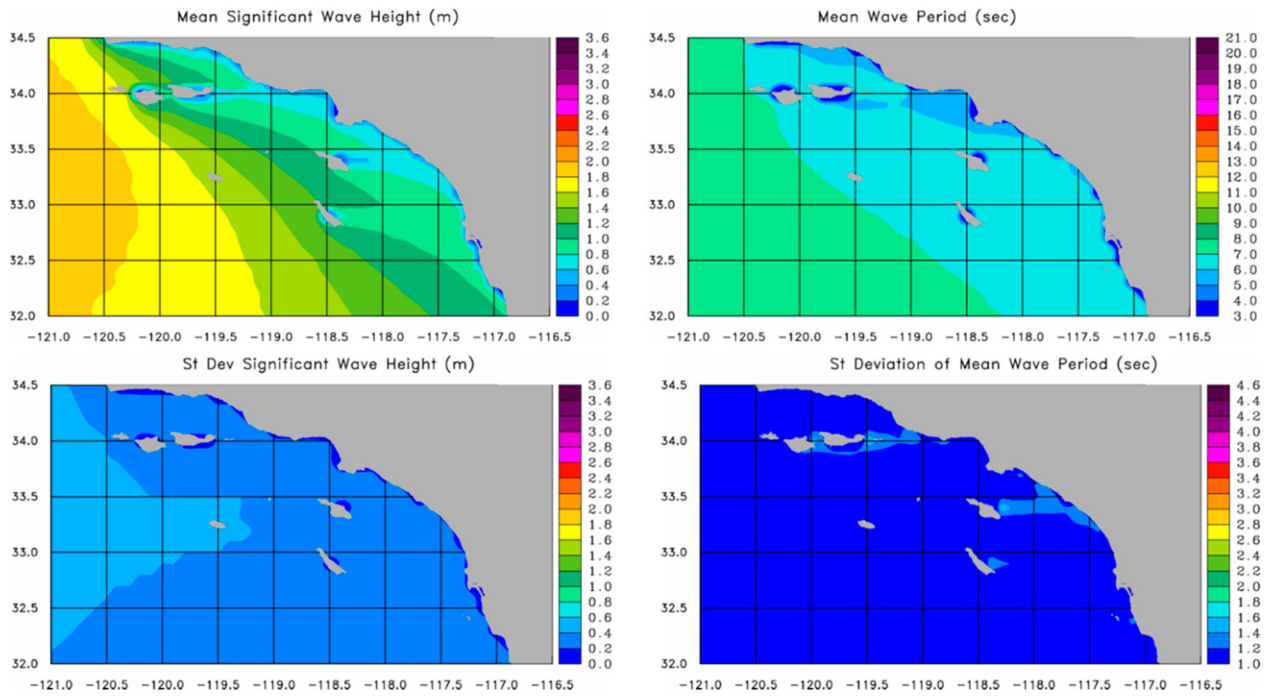


Figure 14. Mean and standard deviation values of the significant wave height and mean wave period for the Summer period (June–August).

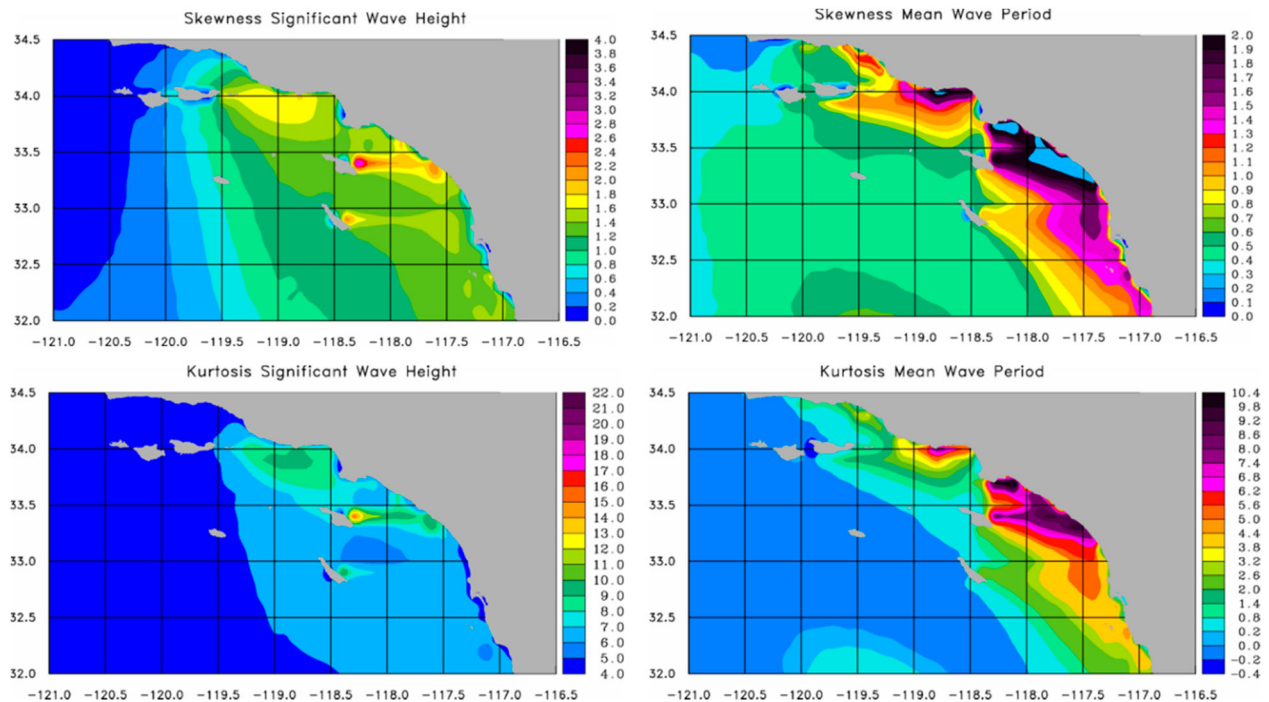


Figure 15. Asymmetry (skewness) and kurtosis measures of the significant wave height and mean wave period for the summer period (June–August).

parameters under study but also for possible asymmetries of the data and the potential impact of extreme values. It should be noted however that the latter concerns the information that could be obtained by the kurtosis (fourth statistical moment) of the data under study

and cannot be considered as a complete extreme value analysis.

For the spring and summer period, increased (up to 2.5 m) H_s values are recorded at the western part of the California islands while shadowing effects

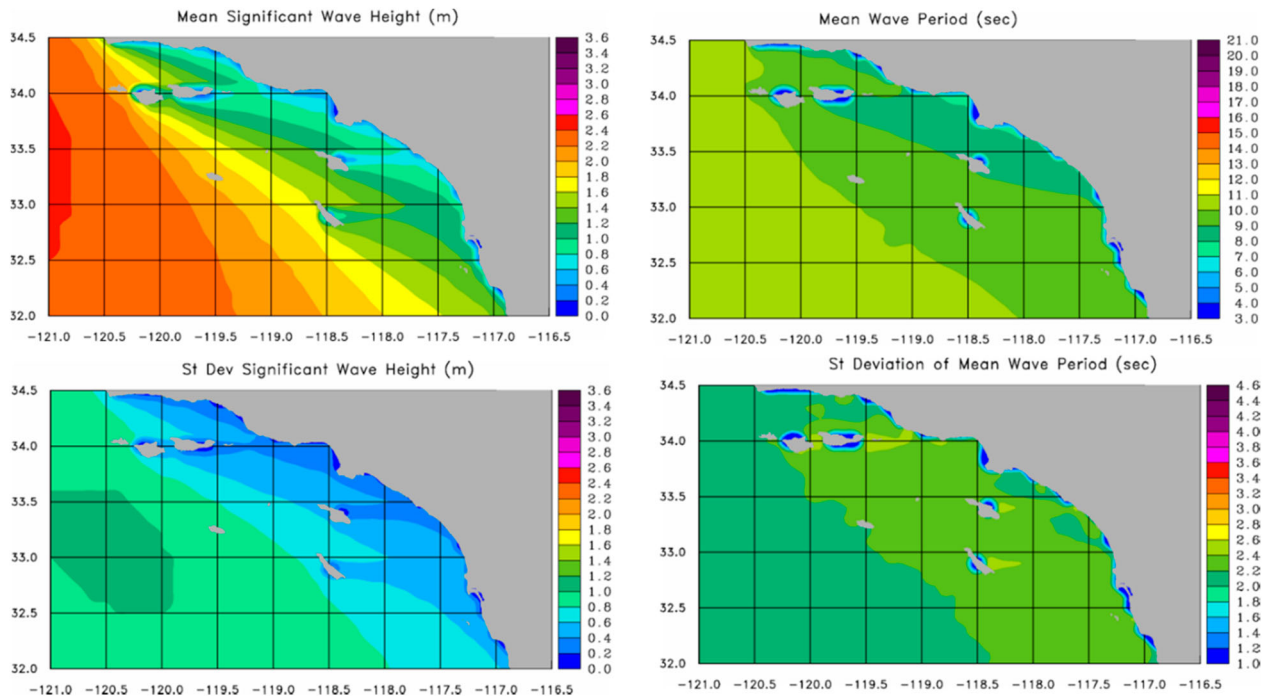


Figure 16. Mean and standard deviation values of the significant wave height and mean wave period for the autumn period (September–November).

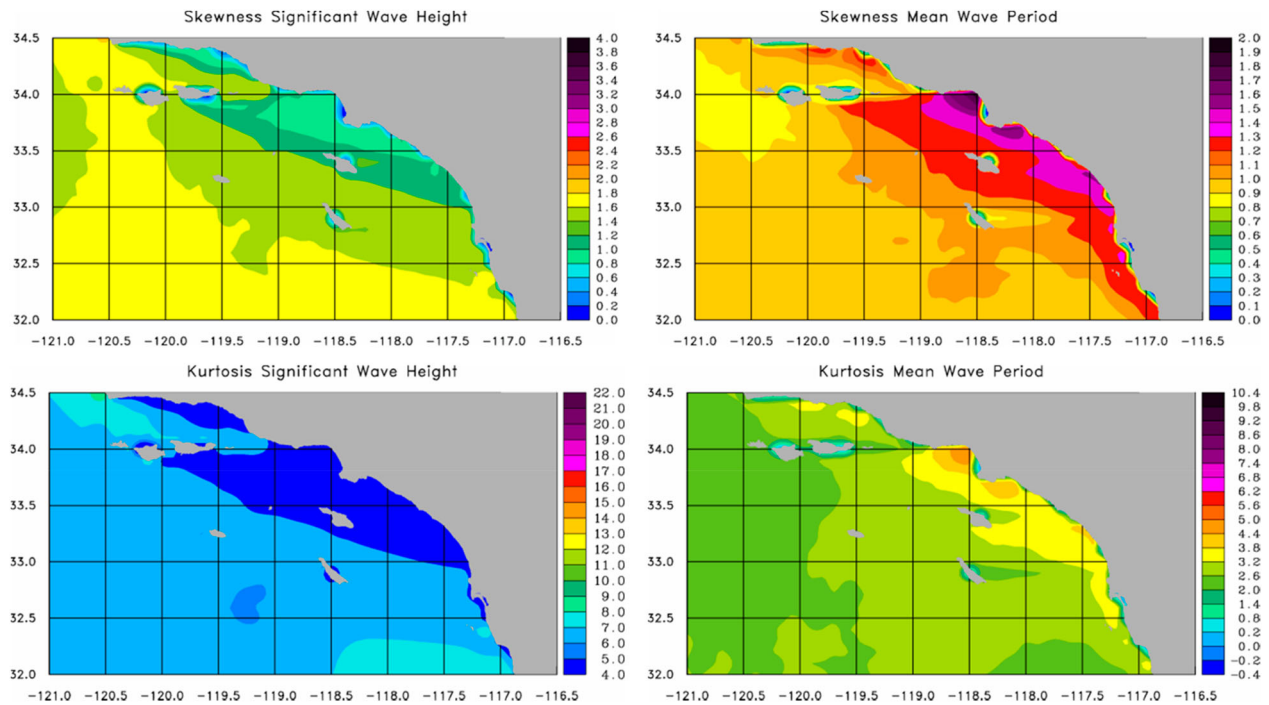


Figure 17. Asymmetry (skewness) and kurtosis measures of the significant wave height and mean wave period for the autumn period (September–November).

appear at the eastern sides. The main component of this consists of long travelled swell waves as the elevated mean wave period values (around 9 s) reveal. On the other hand, mild standard deviations underline

the smooth – with no surprises – wave evolution, another result of the prevailing swell wave component. Asymmetry problems are present only near the coastline.

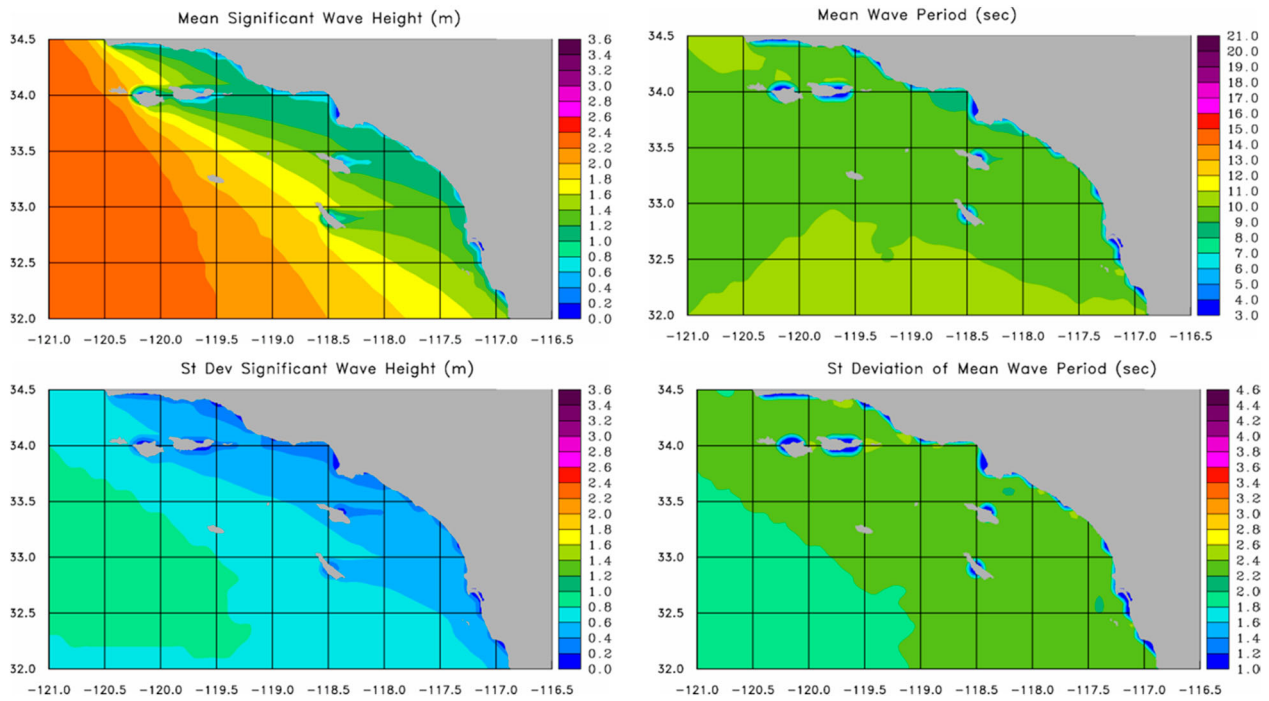


Figure 18. Mean and standard deviation values of the significant wave height and mean wave period for the winter period (December–February).

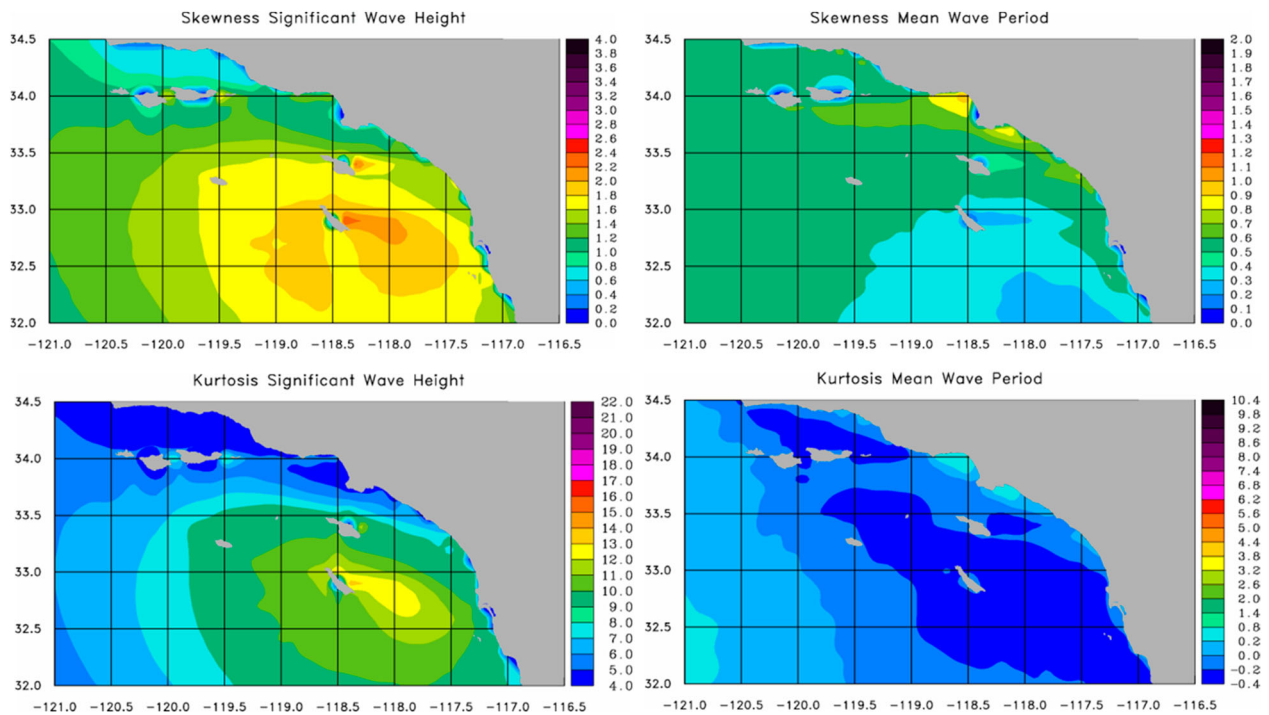


Figure 19. Asymmetry (skewness) and kurtosis measures of the significant wave height and mean wave period for the winter period (December–February).

Increased H_s values ranging between 1 and 3 m are emerging during autumn and winter months (Figures 18 and 19) while swell waves are prevailing (period

~10 s). Some hints of asymmetry are present but in low levels comparing to the expected significant wave height and period values.

These wave characteristics lead to considerable wave energy potential especially over the western coastline of the California islands in a yearly basis with values ranging

between 7 and 25 kW/m during the spring and summer months and reaching 30 kW/m during the most energetic autumn-winter period (Figures 20 and 21).

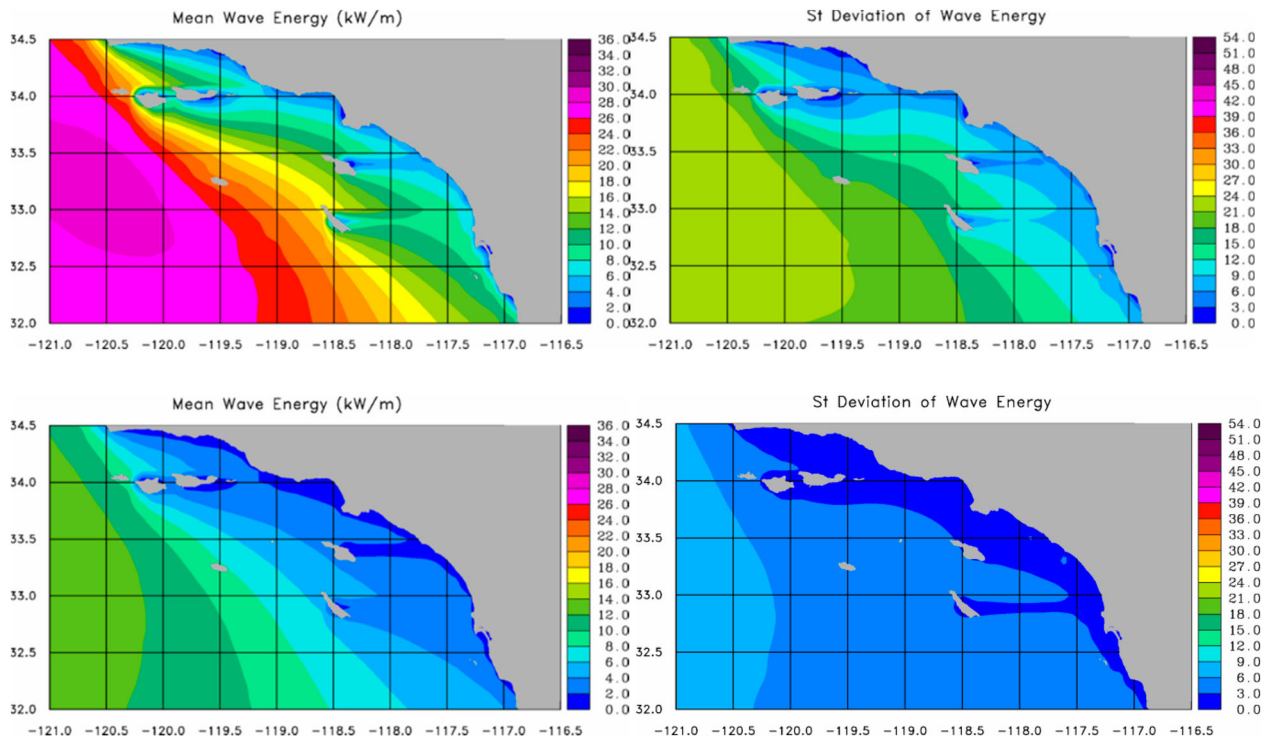


Figure 20. Mean and standard deviation values of wave energy potential for the spring (above) and summer (below) period.

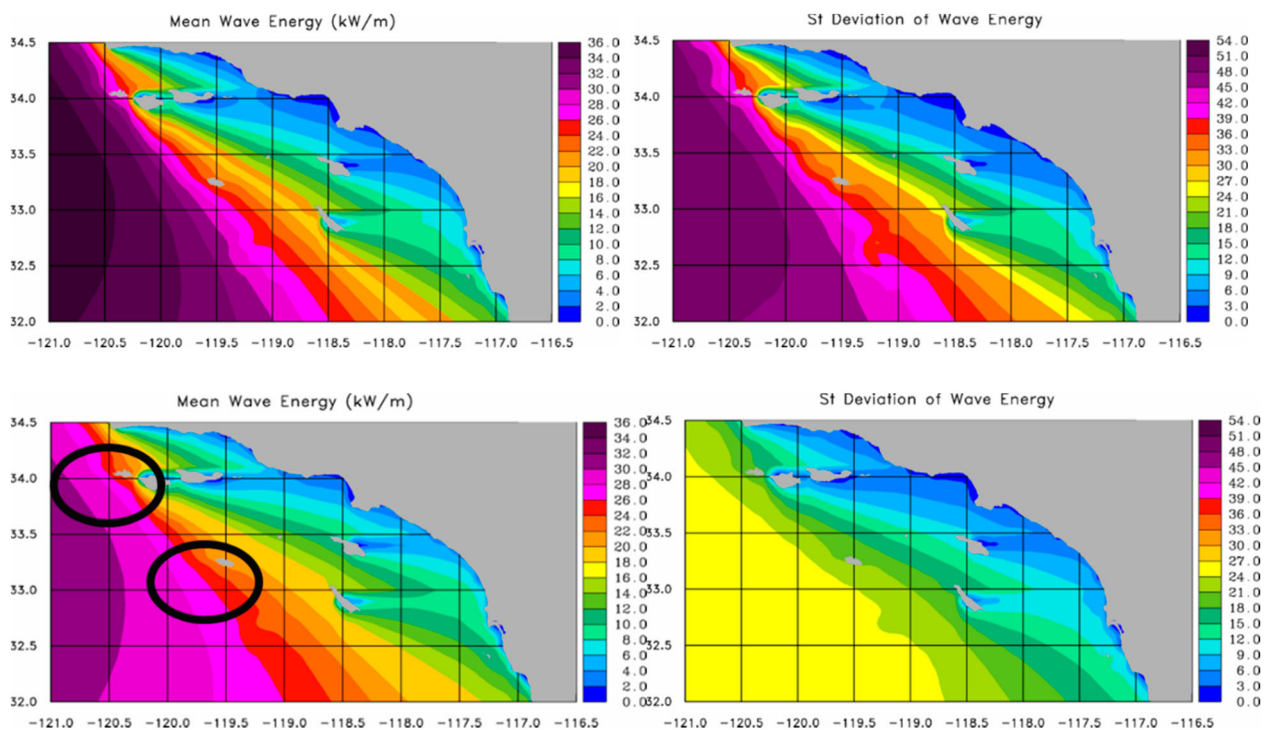


Figure 21. Mean and standard deviation values of wave energy potential for the autumn (above) and winter (below) period.

The most attractive areas for wave energy investments seem to be, by far, the western coastlines of California islands and especially that of Channel and San Nicolas islands. The wave energy potential in there exceeds 30 kW/m especially during autumn and winter months, while the prevailing swell waves ensure the availability of critical wave energy amounts through the whole year, even in periods with low local winds. Moreover, the energy estimated data have low values of asymmetry and kurtosis indices a fact ensuring limited impact of possible extreme events. It should be noted however that wave energy technology is not yet in the mature level of other renewable energy resources and therefore its economic viability is under question. One of the advantages of California compared to other locations is that the wave energy is available closer to the shore, making it cheaper to install and maintain. This further underlines the interest for the California islands spotted above, where the commercial viability of new wave parks development could be supported by the proximity of areas with increased wave energy potential to the land.

5. Conclusions

A new fully operational atmospheric/wave modelling system for the offshore area of the west coastline of the US is presented in this work with special emphasis to the California coastline. This is a result of a joint work of the Naval Ocean Analysis and Prediction Laboratory of the US Naval Postgraduate School; the Center of Excellence in Earth Systems Modeling & Observations of the Schmid College of Science & Technology, Chapman University, Orange, California and the Mathematical Modeling Laboratory of the Naval Academy of Greece.

The operational system consists of two state-of-the-art, widely used numerical models: The atmospheric model RAMS and the wave model WAM, operating at a high horizontal resolution mode towards a 2 km grid in the finest grid of a nested domains sequence. The numerical models are further supported by a new hybrid optimisation post-process, based on non-linear Kalman and Bayesian inference, able to eliminate possible local systematic biases and to critically reduce forecasts uncertainty.

The above system has been evaluated over a period of five years against a wide number of NDBC buoys covering all the latitude range of the west US coastline and focusing on three main parameters, selected for their impact on a number of applications including renewable energy assessment: the wind speed, significant wave height and peak wave period. The results obtained were satisfactory, resulting in very low mean biases of

10^{-2} magnitude and analogously limited RMSE and normalised bias indices. Moreover, it has been proved that for the vast majority of the stations used (more than 80%) the overall deviation of the modelled outputs is less than 10%. Some isolated incidents of elevated discrepancies have been recorded for extreme cases estimation, but even in these cases the deviations were limited to a range between 2% and 10% for the majority of the evaluation stations.

The proposed operational system is already utilised as a monitoring and forecasting tool in the greater area of California but is, furthermore, exploited for a number of applications, including renewable energy activities. Such a case is presented in the third part of the current work focusing to the wave energy potential: the amount of energy that can be produced by the sea waves over the California coastline. The latter proves to be an advantageous area for similar applications, being exposed to long fetch swell waves of the Pacific Ocean that lead to energy potential amounts exceeding 30 kW/m over hot spot areas, some of them a lot close to islands, which is advantageous for installation and maintenance purposes. Moreover, low corresponding impact from extreme values is present and the wave energy data are exposed to limited variability, facts that reveal critical advantages for wave energy platforms development. In this way, ‘clean’ energy production can be pursued at amounts even higher than the analogous cases of the Atlantic European coastline where increased similar activity has already taken place.

Disclosure statement

No potential conflict of interest was reported by the authors.

ORCID

Evgenia Papageorgiou  <http://orcid.org/0000-0002-8968-3228>

Aristotelis Liakatas  <http://orcid.org/0000-0003-4006-8504>

References

- Akpınar A, Kömürcü M. 2013, Jan. Assessment of wave energy resource of the Black Sea based on 15-year numerical hind-cast data. *Appl Energy*. 101:502–512.
- Astitha M, Kallos G, Mihalopoulos N. 2005. Analysis of air quality observations with the aid of the source-receptor relationship approach. *J Air Waste Manag Assoc*. 55:523–535.
- Balis D, Amiridis V, Kazadzis S, Papayannis A, Tsaknakis G, Tzortzakis S, Kalivitis N, Vrekoussis M, Kanakidou M, Mihalopoulos N, et al. 2006. Optical characteristics of desert dust over the East Mediterranean during summer: a case study. *Ann Geophys*. 24:807–821.

- Bernardo J, Smith A. 2000. Bayesian theory. West Sussex: Wiley.
- Bidlot J-R. 2012. Present status of wave forecasting at ECMWF. Proceedings from the ECMWF Workshop on Ocean Waves; June 25–27. Reading: ECMWF.
- Bidlot J-R, Janssen P, Abdalla S, Hersbach H. 2007. A revised formulation of ocean wave dissipation and its model impact. Reading: ECMWF; p. 27. ECMWF Tech. Memo. 509. <http://www.ecmwf.int/publications/>.
- Box G, Tiao G. 1992. Bayesian inference in statistical analysis. New York: Wiley.
- Cotton WR, Pielke RA Sr, Walko RL, Liston GE, Tremback CJ, Jiang H, McAnelly RL, Harrington JY, Nicholls ME, Carriro GG, et al. 2003. RAMS 2001: current status and future directions. *Meteorol Atmos Phys.* 82:5–29.
- Crochet P. 2004. Adaptive Kalman filtering of 2-metre temperature and 10-metre wind-speed forecasts in Iceland. *Meteorol Appl.* 11:173–187.
- Dailey M, Hill B, Lansing N. 1974. A summary of knowledge of the Southern California coastal zone and offshore areas. Vol. I, Physical environment. United States Department of the Interior, Bureau of the Land Management.
- Defne Z, Haas K, Fritz H. 2009. Wave energy potential along the Atlantic coast of the southeastern USA. *Renew Energy.* 34:2197–2205.
- Emmanouil G, Galanis G, Kallos G. 2006. Statistical methods for the prediction of night-time cooling and minimum temperature. *Meteorol Appl.* 13(2):169–178.
- Emmanouil G, Galanis G, Kallos G. 2012. Combination of statistical Kalman filters and data assimilation for improving ocean waves analysis and forecasting. *Ocean Model.* 59–60:11–23.
- Emmanouil G, Galanis G, Kalogeris C, Zodiatis G, Kallos G. 2016. 10-year high resolution study of wind, sea waves and wave energy assessment in the Greek offshore areas. *Renew Energy.* 90:399–419.
- Ferreira JA, Soares CG. 1999. Modelling distributions of significant wave height. *Coast Eng.* 40:361–374.
- Galanis G, Anadranistakis M. 2002. A one dimensional Kalman filter for the correction of near surface temperature forecasts. *Meteorol Appl.* 9:437–441.
- Galanis G, Chu PC, Kallos G. 2011. Statistical post processes for the improvement of the results of numerical wave prediction models. A combination of Kolmogorov-Zurbenko and Kalman filters. *J Oper Oceanogr.* 4(1):23–31.
- Galanis G, Emmanouil G, Kallos G, Chu PC. 2009. A new methodology for the extension of the impact in sea wave assimilation systems. *Ocean Dyn.* 59(3):523–535.
- Galanis G, Hayes D, Zodiatis G, Chu PC, Kuo YH, Kallos G. 2012. Wave height characteristics in the Mediterranean Sea by means of numerical modeling, satellite data, statistical and geometrical techniques. *Mar Geophys Res.* 33:1–15.
- Galanis G, Louka P, Katsafados P, Kallos G, Pytharoulis I. 2006. Applications of Kalman filters based on non-linear functions to numerical weather predictions. *Ann Geophys.* 24:2451–2460.
- Galanis G, Papageorgiou E, Liakatas A. 2017. A hybrid Bayesian Kalman filter and applications to numerical wind speed modeling. *J Wind Eng Ind Aerodyn.* 167:1–22.
- Harvey HT, Nelson PA. 2008. Developing wave energy in California: potential socio-economic effects. California Energy Commission Contract No. 500–07–036.
- Iglesias G, Carballo R. 2009. Wave energy resource along the Death Coast (Spain). *Renew Energy.* 34:1963–1975.
- Iglesias G, Carballo R. 2010. Wave energy resource in the Estaca de Bares area (Spain). *Renew Energy.* 35:1574–1584.
- Iglesias G, Lopez M, Carballo R, Castro A, Fraguera JA, Frigaard P. 2009. Wave energy potential in Galicia (NW Spain). *Renew Energy.* 34:2323–2333.
- Janeiro J, Martins F, Relvas P. 2012. Towards the development of an operational tool for oil spills management in the Algarve coast. *J Coast Conserv.* 16(4):449–460.
- Janjic ZI. 1994. The step-mountain eta coordinate model: further developments of the convection, viscous sublayer, and turbulence closure schemes. *Mon Weather Rev.* 122:927–945.
- Janssen P. 2000. ECMWF wave modeling and satellite altimeter wave data. In: Halpern D, editor. *Satellites, oceanography and society.* New York: Elsevier; p. 35–36.
- Janssen P. 2004. *The interaction of ocean waves and wind.* Cambridge: Cambridge University Press; p. 300.
- Janssen P, Onorato M. 2007. The intermediate water depth limit of the Zakharov Equation and consequences for wave prediction. *J Phys Oceanogr.* 37:2389–2400.
- Kallos G, Lagouvardos K. 1997. Atmospheric modeling simulations over the eastern USA with the RAMS3b model for the summer 1995. Final Report to Electric Power Research Institute, Palo Alto, CA; p. 69.
- Kalman RE. 1960. A new approach to linear filtering and prediction problems. *Trans ASME Ser D.* 82:35–45.
- Kalman RE, Bucy RS. 1961. New results in linear filtering and prediction problems. *Trans ASME Ser D.* 83:95–108.
- Kalnay E. 2002. *Atmospheric modeling, data assimilation and predictability.* Cambridge: Cambridge University Press; p. 341.
- Komen G, Cavaleri L, Donelan M, Hasselmann K, Hasselmann S, Janssen P. 1994. *Dynamics and modelling of ocean waves.* Cambridge: Cambridge University Press.
- Louka P, Galanis G, Siebert N, Kariniotakis G, Katsafados P, Pytharoulis I, Kallos G. 2008. Improvements in wind speed forecasts for wind power prediction purposes using Kalman filtering. *J Wind Eng Ind Aerodyn.* 96:2348–2362.
- Mass CF, Ovens D, Westrick K, Colle BA. 2002. Does increasing horizontal resolution produce more skillful forecasts? *Bull Am Meteorol Soc.* 83(3):407–430.
- Mavromatidis E, Kallos G. 2002. A study of cold and warm cloud formation with RAMS. Atmospheric modelling from microscale to global, 5th RAMS workshop and related applications; 30 September–3 October 2002; Santorini, Greece.
- Mori N, Janssen PAEM. 2006. On kurtosis and occurrence probability of freak waves. *J Phys Oceanogr.* 36:1471–1483.
- Nickovic S, Kallos G, Papadopoulos A, Kakaliagou O. 2001. A model for prediction of desert dust cycle in the atmosphere. *J Geophys Res.* 106(D16):18113–18129.
- Papadopoulos A, Kallos G, Katsafados P, Nickovic S. 2002. The POSEIDON weather forecasting system: an overview. *Glob Atmos Ocean Syst.* 8:219–237.
- Papadopoulos A, Katsafados P. 2009. Verification of operational weather forecasts from the POSEIDON system across the Eastern Mediterranean. *Nat Hazards Earth Syst Sci.* 9:1299–1306.
- Pelland S, Galanis G, Kallos G. 2011. Solar and photovoltaic forecasting through post-processing of the global environmental multiscale numerical weather prediction model. *Prog Photovolt Res Appl.* DOI:10.1002/pip.1180

- Rao ST, Zurbenko IG, Neagu R, Porter PS, Ku JY, Henry RF. 1997. Space and time scales in ambient ozone data. *Bull Am Meteorol Soc.* 78(10):2153–2166.
- Rusu L, Soares G. 2012. Wave energy assessments in the Azores islands. *Renew Energy.* 45:183–196.
- Spyrou C, Mitsakou C, Kallos G, Louka P, Vlastou G. 2010. An improved limited area model for describing the dust cycle in the atmosphere. *J Geophys Res.* 115(17). D17211. DOI:10.1029/2009JD013682
- WAMDIG, The WAM-Development and Implementation Group: Hasselmann S, Hasselmann K, Bauer E, Bertotti L, Cardone CV, Ewing JA, Greenwood JA, Guillaume A, Janssen P, Komen G, et al. 1988. The WAM Model - a third generation ocean wave prediction model. *J Phys Oceanogr.* 18(12):1775–1810.
- Stathopoulos C, Kaperoni A, Galanis G, Kallos G. 2013. Wind power prediction based on numerical and statistical models. *J Wind Eng Ind Aerodyn.* 112:25–38.
- Zodiatis G, Galanis G, Kallos G, Nikolaidis A, Kalogeri C, Liakatas A, Stylianos S. 2015. The impact of sea surface currents in wave power potential modelling. *Ocean Dyn.* 65:1547–1565.
- Zodiatis G, Galanis G, Nikolaidis A, Kalogeri C, Hayes D, Georgiou G, Chu PC, Kallos G. 2014. Wave energy potential in the eastern Mediterranean Levantine Basin. An integrated 10-year study. *Renew Energy.* 69:311–323.
- Zodiatis G, Lardner R, Georgiou G, Demirov E, Manzella G, Pinardi N. 2003. An operational European global ocean observing system for the eastern Mediterranean Levantine Basin: the Cyprus coastal ocean forecasting and observing system. *Mar Technol Soc J.* 37(3):115–123.
- Zodiatis G, Lardner R, Hayes D, Georgiou G, Sofianos S, Skliris N, Lascaratos A. 2008. Operational ocean forecasting in the Eastern Mediterranean: implementation and evaluation. *Ocean Sci.* 4(1):31–47.